

# Conformal data and renormalization group flow in critical quantum spin chains using periodic uniform matrix product states

Yijian Zou,<sup>\*</sup> Ashley Milsted,<sup>†</sup> and Guifré Vidal

*Perimeter Institute for Theoretical Physics, Waterloo ON, N2L 2Y5, Canada*

(Dated: January 15, 2022)

We propose and demonstrate the use of periodic uniform Matrix Product States (puMPS) to extract conformal data from a critical quantum spin chain and to study its RG flow non-perturbatively. Given a microscopic lattice Hamiltonian, its ground state is approximated by a puMPS, whereas low energy excited states are approximated as puMPS Bloch states. Conformal data is then extracted from these low energy states by computing the energy-momentum spectra and from matrix elements of the (Koo-Saleur) lattice Virasoro generators, as recently outlined in [Milsted, Vidal, arXiv:1706.01436]. The *spectral* RG flow is studied by monitoring the low-energy spectrum of a fixed microscopic Hamiltonian for a sequence of increasingly large chains, ranging from a few spins to several hundred spins. As an example we consider a flow in the Axial Next-Nearest-Neighbor Ising (ANNNI) model that mimics the RG flow interpolating between the Tri-Critical Ising CFT in the UV and the Ising CFT in the IR.

Near a continuous phase transition, microscopically different systems may display strikingly similar long-distance behavior – that is, they belong to the same critical universality class [1]. In the language of the renormalization group (RG), which describes how physics changes with scale, such systems are said to “flow” to the same scale-invariant theory or RG fixed point. These fixed points are often described by a conformal field theory (CFT) [2, 3], which may in turn be specified by a set of parameters known as conformal data.

Given a microscopic description of a critical system (e.g. in terms of a lattice Hamiltonian), an important, yet challenging task is to extract the conformal data as a means to identify the universality class of the phase transition. For critical quantum spin chains – the focus of this work – much progress can be made in highly fine-tuned models, such as integrable lattice models (for example, [4–10]). However, for a generic spin chain Hamiltonian one must resort to numerical methods. Exact diagonalization (ED) techniques are useful [11, 12], but can only deal with small systems, where the long-distance, universal physics is often significantly obscured by the non-universal, microscopic details. Monte Carlo methods can address much larger systems [13], but only in models that do not suffer from the sign problem. On the other hand, tensor network methods [14–16] are both sign-problem free and scalable, and several schemes have been proposed to extract conformal data [17–22]. These include schemes [17–19, 21] based on the matrix product state (MPS) [15, 23], which is the ansatz underlying the density matrix renormalization group (DMRG) algorithm [14, 24].

In this Letter we propose and demonstrate the use of periodic uniform Matrix Product States (puMPS) [25] to extract conformal data from critical quantum spin chains on the circle. We show that, by explicitly preserving translation invariance, this ansatz provides an accurate, scalable approximation to both the ground state

and the low-energy excited states of a critical quantum spin chain. Considering periodic chains of up to several hundreds of spins, we can then extract conformal data from these states by using both the energy-momentum spectrum [26–29] and the matrix elements of lattice Virasoro generators [12, 30]. Finally, we apply this formalism to a critical spin model that interpolates between the Ising and Tri-Critical Ising (TCI) universality classes, enabling us to accurately track the low energy excitations along (a lattice analogue of) the RG flow between the two corresponding CFT’s.

*Matrix Product State ansatz.* A puMPS [25]  $|\Psi(A)\rangle \equiv \sum_{\vec{s}=1}^d \text{tr}(A^{s_1} A^{s_2} \dots A^{s_N}) |\vec{s}\rangle$ , where  $\vec{s} = s_1 \dots s_N$  and  $d$  is the Hilbert-space dimension of one lattice site, is specified by a tensor  $A_{ab}^s$  of dimension  $d \times D \times D$ , together with the number of sites  $N$ . The *bond dimension*  $D$  controls the amount of *entanglement* in the state ( $D^2$  is the maximum Schmidt rank of a bipartition of the system). To approximate the ground state of a local Hamiltonian  $H$  within the variational class of puMPS we use a gradient descent method, analogous to that employed in [31], with the norm  $\eta$  of the local gradient  $|\Gamma\rangle$  (also an MPS) used to determine convergence. See [32] for details.

Once we have a puMPS that approximates the ground state, we seek excitations within the space of puMPS *Bloch states* [33, 34], which have the form

$$|\Phi_p(B)\rangle \equiv \sum_{j=1}^N e^{-ipj} T^j \sum_{\vec{s}=1}^d \text{tr}(B^{s_1} A^{s_2} \dots A^{s_N}) |\vec{s}\rangle, \quad (1)$$

where  $T$  is the translation operator,  $p$  is the momentum,  $A$  is the ground-state puMPS tensor, and  $B_{ab}^s$  parameterizes a Bloch state. To find excitations we must solve a generalized eigenvalue problem, the conditioning of which we can improve by an appropriate gauge choice (a form of preconditioning) [32].

*Extracting conformal data.* Given (approximate) excited states of a critical circular spin chain, we wish to

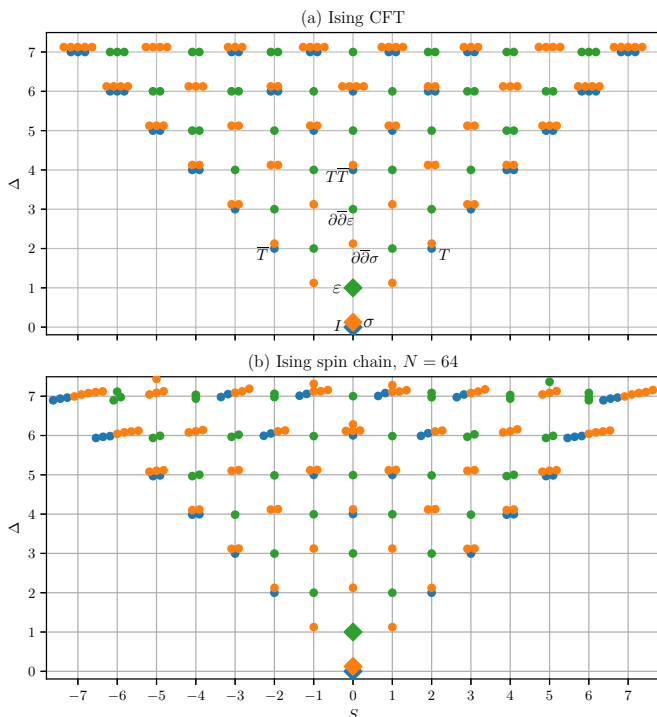


Figure 1. (a) Exact Ising CFT scaling operator spectrum, with diamonds marking primary operators. (b) Ising model spectrum, colored according to numerical conformal-tower identification, for  $N = 64$  sites using Bloch states on top of a puMPS variational ground state with  $D = 24$ , converged to  $\eta < 10^{-6}$  (error on ground-state energy density  $\approx 10^{-11}$ ). The numerically-assigned conformal towers are consistent with the CFT result up to level 7, where some states are misidentified. **Note:** We displace data points slightly in the x-direction to show degeneracies.

extract conformal data of the 2D CFT describing its RG fixed point. This includes [2] the *scaling dimensions*  $\Delta_\alpha$  and *conformal spins*  $S_\alpha$  of certain *scaling operators* (field operators that are covariant under dilations)  $\phi_\alpha$  called *primary fields*, and the *central charge*  $c$ . There are several useful results [26–30, 35–37] that relate accessible finite-size quantities to this conformal data. Here we make use of the discovery [26–29] that the eigenstates of  $H$  have energies  $E_\alpha$  and momenta  $P_\alpha$  given by

$$E_\alpha = A + B \frac{2\pi}{N} \left( \Delta_\alpha - \frac{c}{12} \right) + O(N^{-x}), \quad P_\alpha = \frac{2\pi}{N} S_\alpha, \quad (2)$$

where  $N$  is the number of spins, and  $A$ ,  $B$ ,  $x$  are constants specific to the microscopic model  $H$ . Up to these constants (2) is just the energy-momentum spectrum of the CFT on the circle, with  $x > 1$  determining subleading corrections to its scaling with  $N$ . The appearance of  $\Delta_\alpha, S_\alpha$  is due to the *operator-state correspondence*: each energy eigenstate corresponds to a scaling operator [2]. To systematically identify the CFT operator that each pair  $\Delta_\alpha, S_\alpha$  correspond to, we apply new methods [12]

that utilize lattice representations [30]

$$H_n = \frac{N}{2\pi} \sum_{j=1}^N e^{ijn\frac{2\pi}{N}} h_j \sim L_n + \bar{L}_{-n}, \quad (3)$$

of the Virasoro generators  $L_n, \bar{L}_n$  of conformal transformations [2]. These act as *ladder operators* on the eigenstates of  $H$ , which are subdivided into multiple *conformal towers* of states, each descended from a distinct primary field state. The operators (3) also provide an estimate of  $c \approx 2|\langle T|H_{-2}|I\rangle|^2$ , where  $|I\rangle$  is the ground state and  $|T\rangle$  an excited state corresponding to the CFT energy-momentum operator.

*Benchmark results.* To use the methods of [12] with variational methods, we not only need accurate excitation energies, the eigenstates of  $H$  must themselves be accurate. As a first test of the puMPS Bloch state ansatz, we thus compute the fidelity of variational excitations with their exact counterparts (found by ED) for the transverse field Ising model  $H = -\sum_{j=1}^N [\sigma_j^X \sigma_{j+1}^X + \sigma_j^Z]$  on  $N = 20$  sites. We find [32] that all excited states corresponding to scaling dimensions  $\Delta < 5$  are representable using (1) at the tested bond dimensions  $D = 6 \dots 16$ . Furthermore, although the accuracy decays exponentially with the energy of the excitation, we can always improve this accuracy by increasing  $D$ .

To test the extraction of conformal data using puMPS Bloch states, we compute many variational excitations for a system of size  $N = 64$  with  $D = 24$ , using (2) to estimate the scaling dimensions of the corresponding CFT scaling operators and then applying an improved version [32] of the algorithm of [12] for assigning states to conformal towers. The result in Fig. 1, all computations for which were carried out in a matter of minutes on a modestly powerful laptop, shows that we obtain excellent accuracy, with misidentification of states occurring only at level 7 (and above). As a further test of accuracy, we compute variational excitations for system sizes up to  $N = 228$  (with  $24 \leq D \leq 36$ ) and extrapolate the scaling dimensions of a selection of scaling operators, as well as central charge (using (3)), to large  $N$ . The results

	Exact value	Numerical value	relative error
$c$	0.5	0.499990	$2 \times 10^{-5}$
$\Delta_\sigma$	0.125	0.1249990	$8 \times 10^{-6}$
$\Delta_\epsilon$	1	0.999994	$6 \times 10^{-6}$
$\Delta_{\partial\bar{\partial}\sigma}$	2.125	2.1253	$1 \times 10^{-4}$
$\Delta_{\partial\bar{\partial}\epsilon}$	3	3.0003	$1 \times 10^{-4}$

compare favorably with those of [21], where infinite MPS are used to determine the central charge and the primary field scaling dimensions, as well as scaling dimensions obtained from MERA and TNR tensor-network techniques [20, 38]. It is also worth noting that the algorithms we use are significantly simpler than those required for the

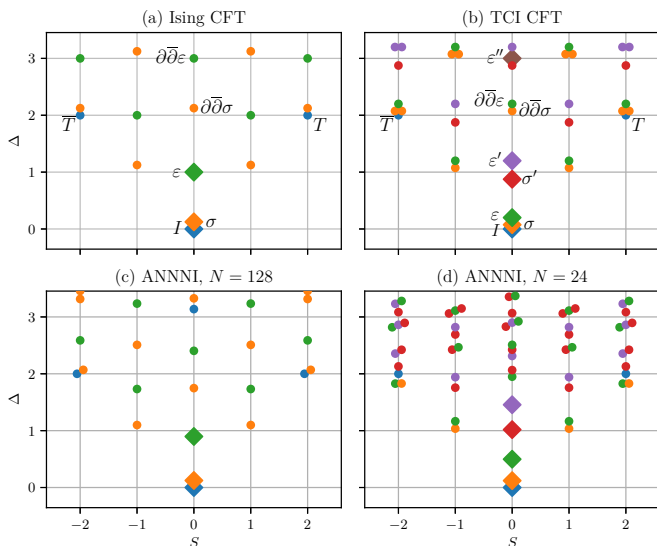


Figure 2. **Top:** Scaling operator spectra of (a) the Ising and (b) the TCI CFT's (with a selection of operators labeled). **Bottom:** Approximate scaling dimensions and conformal-tower identification for the ANNNI model at  $\delta = 10$  with (c)  $N = 128, D = 46$  and (d)  $N = 24, D = 24$ , corresponding to the left-most and right-most points of Fig. 3, respectively.

mentioned methods, despite being somewhat more complicated than DMRG.

*Spectral RG flow.* We now turn to the ANNNI (Axial Next-Nearest-Neighbor Ising) model

$$H = - \sum_{j=1}^N [\sigma_j^X \sigma_{j+1}^X + \sigma_j^Z + \gamma (\sigma_j^X \sigma_{j+2}^X + \sigma_j^Z \sigma_{j+1}^Z)],$$

which includes the critical Ising model at  $\gamma = 0$  and features a Tri-Critical Ising (TCI) point at  $\gamma_{\text{TCI}} \approx 247$  [39]. It is symmetric under  $\sigma^X \rightarrow -\sigma^X$  and is self dual for all  $\gamma$  [40, 41]. For our purposes this is an interesting model because the  $\gamma$  term is the lattice analogue of the  $T\bar{T}$  operator (and higher- $\Delta$  descendants) in the Ising CFT, and the relevant primary operator  $\varepsilon'$  ( $\phi_{1,3}$  in the Kac table) in the TCI CFT. This can be confirmed by computing the matrix elements of the  $\gamma$  term in the low-energy eigenbasis of  $H$  at the Ising ( $\gamma = 0$ ) and TCI points. The interpolating flow between the TCI and the Ising CFT's via this operator has been studied in integrable field theory [42–44] and also using the truncated CFT Hilbert space approach [45, 46], as well as in integrable lattice models [5, 6, 47]. Here, we study the flow non-perturbatively in a nonintegrable lattice model using methods that can be applied to any spin-chain system. To do this, we compute the low-energy spectrum of the ANNNI model, scaled and shifted so that the ground state has  $E = \Delta_I = 0$  and  $|T\rangle$  has  $E = \Delta_T = 2$  (see [12]), as a function of two parameters:  $N$  and  $\gamma$ .

We call the flow with  $N$  a *spectral* RG flow [48] to emphasize that we are studying the flow of the low-energy

spectrum, rather than the couplings of an effective Hamiltonian. How should we expect the spectral RG flow to look? If we consider the ANNNI model at finite  $N$  with  $\gamma = \gamma_{\text{TCI}} - \delta$  (for small  $\delta > 0$ ) to be a relevant deformation of the TCI CFT then the low-energy physics will be dominated by the nearby TCI point at small  $N$ , while increasing  $N$  will eventually reveal the Ising CFT. It turns out we can even observe this flow at  $\gamma = 10$ , where in Fig. 2 we see that the low-energy excitations spectrum at  $N = 24$  exhibits some striking similarities to the TCI CFT spectrum, while at  $N = 128$  it looks like the Ising CFT spectrum. Also in Fig. 2, we show conformal tower membership computed using (3). At  $N = 24$ , despite strong corrections due to the relevant  $\varepsilon'$  perturbation, and further irrelevant perturbations, we nevertheless reproduce some of the low-lying tower-membership results of the TCI. At large  $N$ , the state identifications correspond well to the Ising CFT.

We plot the spectral RG flow at  $\gamma = 10$  for a selection of states in Fig. 3, including those that would correspond to primary operators in the TCI CFT. We find we can easily determine which Ising CFT operators the TCI CFT primaries correspond to, allowing us to identify:

$$\begin{array}{c|c|c|c|c|c} \text{TCI operator} & I & \sigma & \varepsilon & \sigma' & \varepsilon' \\ \hline \text{Ising operator} & I & \sigma & \varepsilon & \partial\bar{\partial}\sigma & T\bar{T} \end{array}$$

These results match those found in other studies of different microscopic realizations of the same CFT's, e.g. [6], and conform with expectations from symmetry considerations. The identity of  $\varepsilon'$  in the TCI CFT with  $T\bar{T}$  in the Ising CFT matches their both being associated with the  $\gamma$  term in  $H$ .

We can better confirm the TCI operator identities of the low-energy states at  $\gamma = 10$  by tracking them as a function of  $\gamma \rightarrow \gamma_{\text{TCI}}$ . This we do in Fig. 4 for fixed  $N = 80$  (to avoid strong irrelevant corrections vs.  $N = 24$  in Fig. 2 (d)). We find a very similar pattern to Fig. 3, which we would expect if the RG flow of Hamiltonian couplings sends  $\gamma$  to zero for any starting  $\gamma < \gamma_{\text{TCI}}$ . Using both plots we can connect the low-energy eigenstates at  $\gamma = 10, N = 128$ , which we identified with Ising CFT operators, with corresponding eigenstates at  $\gamma = 100, N = 80$ , which we can confidently match up with TCI CFT operators.

*Summary and conclusions.* We have proposed and demonstrated the use of puMPS and puMPS Bloch states for extraction of conformal data from critical spin chains. The ability to compute accurate variational low-energy eigenstates at large system sizes (far beyond the reach of ED) using these techniques enabled us to study a spectral RG flow in the self-dual ANNNI model, allowing us to identify low-energy eigenstates with CFT operators in both the Ising and Tri-Critical Ising CFT's.

We remark that it was *a priori* far from obvious that puMPS Bloch states should be an appropriate ansatz for extracting conformal data since, in a generic spin chain, multiparticle scattering states necessitate the use of a

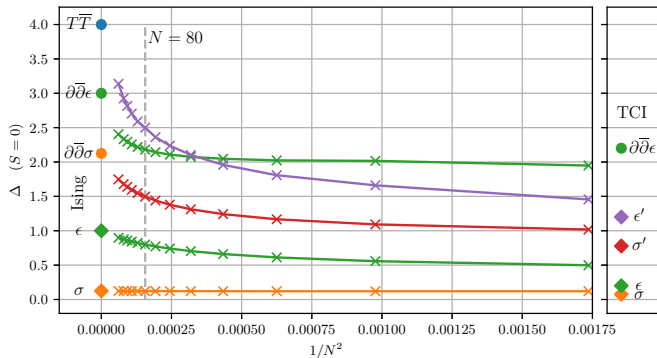


Figure 3. Spectral RG flow of the first 5 approximate scaling dimensions (crosses), excluding  $\Delta = 0$ , extracted from the ANNNI model at momentum zero, for  $\gamma = 10$ , using  $D \leq 46$ . For comparison, we also plot the exact scaling dimensions of the Ising and TCI CFT’s. Note the crossover between the two largest scaling dimensions plotted, which we confirm by also tracking the  $\varepsilon$ -tower membership using  $H_n$  matrix elements.

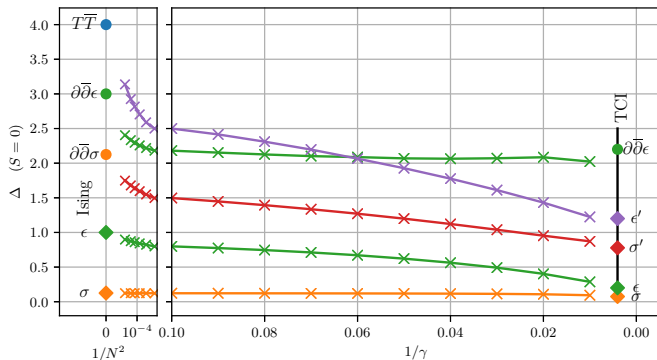


Figure 4. The first 5 approximate scaling dimensions (crosses), excluding  $\Delta = 0$ , as function of  $\gamma$ , extracted from the ANNNI model at momentum zero, for  $N = 80, D = 38$ . We also plot exact CFT scaling dimensions. Furthermore, we show to the left how the “flow” with  $\gamma$  links up at  $\gamma = 10$  with the spectral RG flow of Fig. 3. We confirm the crossover between the two highest- $\Delta$  curves by tracking fidelities of excited states at different  $\gamma$ .

modified ansatz [49] for all but the lowest-energy excited states [50].

However, excited states in the CFT can be created by acting on the vacuum with a linear combination of Fourier modes of field operators [51, 52], making Bloch states an apparently good match. Furthermore, in a critical system (for sufficiently large  $D$  [53]) correlations in the puMPS are long range so that the tensor  $B$  of (1) is well-positioned to capture the action on the ground state of operators that act nontrivially on large segments of the chain, as the lattice analogues of field operators may do in case of higher derivatives  $\partial_x^m \phi(x)$ .

Certainly we observe that variational low-energy excitations can be computed using Bloch states with sufficient accuracy to allow accurate assignment of conformal

towers, and computation of the central charge, using Koo-Saleur lattice Virasoro generators [12, 30]. This is strong confirmation of the suitability of the Bloch state ansatz. Note also that the ansatz can easily be improved by considering  $B$  tensors that encompass two or more lattice sites, instead of one [54].

Finally, we comment on the benefits of dealing with variational states that are exact momentum eigenstates. Not only does this give us precise values for the conformal spin via (2), it allows us to easily distinguish higher-level eigenstates that might be difficult to obtain using methods that sacrifice spatial uniformity. For example, it is easy to obtain the state  $|T\rangle$ , which has  $\Delta = 2, S = 2$  and is typically used to determine the scaling factor needed to translate scaling dimensions into energies [12, 55]. This is difficult using DMRG, where alternative methods for computing the scaling factor are preferred [19].

*Acknowledgments.* We thank Martin Ganahl for many useful discussions, as well as Jutho Haegeman and Frank Verstraete for valuable comments. The authors acknowledge support from the Simons Foundation (Many Electron Collaboration) and Compute Canada. Research at Perimeter Institute is supported by the Government of Canada through Industry Canada and by the Province of Ontario through the Ministry of Research and Innovation.

\* yzhou@pitp.ca

† amilsted@pitp.ca

- [1] K. G. Wilson and J. Kogut, *Phys. Rep.* **12**, 75 (1974).
- [2] A. A. Belavin, A. M. Polyakov, and A. B. Zamolodchikov, *Nucl. Phys. B* **241**, 333 (1984).
- [3] D. Friedan, Z. Qiu, and S. Shenker, *Phys. Rev. Lett.* **52**, 1575 (1984).
- [4] A. B. Zamolodchikov, *Nucl. Phys. B* **358**, 497 (1991).
- [5] G. Feverati, P. A. Pearce, and F. Ravanini, *Physics Letters B* **534**, 216 (2002), arXiv:hep-th/0202041.
- [6] P. A. Pearce, L. Chim, and C. Ahn, *Nuclear Physics B* **660**, 579 (2003), arXiv:hep-th/0302093.
- [7] N. Read and H. Saleur, *Nucl. Phys. B* **777**, 263 (2007), arXiv:cond-mat/0701259.
- [8] A. M. Gainutdinov and R. Vasseur, *Nucl. Phys. B* **868**, 223 (2013), arXiv:1203.6289.
- [9] R. Bondesan, J. Dubail, A. Faribault, and Y. Ikhlef, *J. Phys. A: Math. Theor.* **48**, 065205 (2015), arXiv:1409.8590.
- [10] M. S. Zini and Z. Wang, (2017), arXiv:1706.08497.
- [11] A. Feiguin, S. Trebst, A. W. W. Ludwig, M. Troyer, A. Kitaev, Z. Wang, and M. H. Freedman, *Phys. Rev. Lett.* **98**, 160409 (2007), arXiv:cond-mat/0612341.
- [12] A. Milsted and G. Vidal, (2017), arXiv:1706.01436.
- [13] A. W. Sandvik, *AIP Conf. Proc.* **1297**, 135 (2010), arXiv:1101.3281.
- [14] S. R. White, *Phys. Rev. Lett.* **69**, 2863 (1992).
- [15] M. Fannes, B. Nachtergaele, and R. F. Werner, *Commun. Math. Phys.* **144**, 443 (1992).
- [16] G. Vidal, *Phys. Rev. Lett.* **99**, 220405 (2007), arXiv:cond-



- mat/0512165.
- [17] C. Degli, E. Boschi, and F. Ortolani, *Eur. Phys. J. B* **41**, 503 (2004).
- [18] L. Tagliacozzo, T. R. de Oliveira, S. Iblisdir, and J. I. Latorre, *Phys. Rev. B* **78**, 024410 (2008), arXiv:0712.1976.
- [19] J. C. Xavier, *Phys. Rev. B* **81**, 224404 (2010), arXiv:1002.0531.
- [20] G. Evenbly and G. Vidal, in *Strongly Correlated Systems*, Springer Series in Solid-State Sciences No. 176, edited by A. Avella and F. Mancini (Springer Berlin Heidelberg, 2013) pp. 99–130, arXiv:1109.5334.
- [21] V. Stojevic, J. Haegeman, I. P. McCulloch, L. Tagliacozzo, and F. Verstraete, *Phys. Rev. B* **91**, 035120 (2015), arXiv:1401.7654.
- [22] G. Evenbly and G. Vidal, *Phys. Rev. Lett.* **115**, 180405 (2015), arXiv:1412.0732.
- [23] G. Vidal, *Phys. Rev. Lett.* **93**, 040502 (2004).
- [24] U. Schollwöck, *Annals of Physics* **326**, 96 (2011).
- [25] B. Pirvu, F. Verstraete, and G. Vidal, *Phys. Rev. B* **83**, 125104 (2011).
- [26] J. L. Cardy, *J. Phys. A: Math. Gen.* **17**, L385 (1984).
- [27] H. W. J. Blöte, J. L. Cardy, and M. P. Nightingale, *Phys. Rev. Lett.* **56**, 742 (1986).
- [28] I. Affleck, *Phys. Rev. Lett.* **56**, 746 (1986).
- [29] J. L. Cardy, *Nucl. Phys. B* **270**, 186 (1986).
- [30] W. M. Koo and H. Saleur, *Nucl. Phys. B* **426**, 459 (1994), arXiv:hep-th/9312156.
- [31] M. Ganahl, J. Rincon, and G. Vidal, (2016), arXiv:1611.03779.
- [32] Supplemental material.
- [33] S. Rommer and S. Östlund, *Phys. Rev. B* **55**, 2164 (1997).
- [34] B. Pirvu, J. Haegeman, and F. Verstraete, *Phys. Rev. B* **85**, (2012), arXiv:1103.2735.
- [35] C. Holzhey, F. Larsen, and F. Wilczek, *Nucl. Phys. B* **424**, 443 (1994), arXiv:hep-th/9403108.
- [36] P. Calabrese and J. Cardy, *J. Stat. Mech.* **2004**, P06002 (2004), arXiv:hep-th/0405152.
- [37] F. C. Alcaraz, M. I. Berganza, and G. Sierra, *Physical Review Letters* **106**, (2011), arXiv:1101.2881.
- [38] M. Hauru, G. Evenbly, W. W. Ho, D. Gaiotto, and G. Vidal, *Phys. Rev. B* **94**, (2016), arXiv:1512.03846.
- [39] A. Rahmani, X. Zhu, M. Franz, and I. Affleck, *Phys. Rev. Lett.* **115**, (2015), arXiv:1504.05192.
- [40] A. Milsted, L. Seabra, I. C. Fulga, C. W. J. Beenakker, and E. Cobanera, *Phys. Rev. B* **92**, (2015), arXiv:1504.07258.
- [41] A. Rahmani, X. Zhu, M. Franz, and I. Affleck, *Phys. Rev. B* **92**, (2015), arXiv:1505.03966.
- [42] D. A. Kastor, E. J. Martinec, and S. H. Shenker, *Nucl. Phys. B* **316**, 590 (1989).
- [43] A. B. Zamolodchikov, *Nucl. Phys. B* **358**, 524 (1991).
- [44] T. R. Klassen and E. Melzer, *Nuclear Physics B* **370**, 511 (1992).
- [45] M. Lässig, G. Mussardo, and J. L. Cardy, *Nucl. Phys. B* **348**, 591 (1991).
- [46] P. Giokas and G. Watts, (2011), arXiv:1106.2448.
- [47] G. Feverati and P. Grinza, *Nucl. Phys. B* **702**, 495 (2004), arXiv:hep-th/0405110.
- [48] Notice that the ratio  $1/N$  of the lattice spacing to the system size can be understood as a UV length scale, hence the flow with  $N$  can be considered an RG flow.
- [49] L. Vanderstraeten, F. Verstraete, and J. Haegeman, *Phys. Rev. B* **92**, 125136 (2015).
- [50] J. Haegeman, S. Michalakis, B. Nachtergaele, T. J. Osborne, N. Schuch, and F. Verstraete, *Phys. Rev. Lett.* **111**, 080401 (2013), arXiv:1305.2176.
- [51] P. Ginsparg, lecture notes (1988), arXiv:hep-th/9108028.
- [52] P. Di Francesco, P. Mathieu, and D. Senechal, *Conformal Field Theory* (Springer, New York, 2012).
- [53] B. Pirvu, G. Vidal, F. Verstraete, and L. Tagliacozzo, *Phys. Rev. B* **86**, 075117 (2012), arXiv:1204.3934.
- [54] J. Haegeman, T. J. Osborne, and F. Verstraete, *Phys. Rev. B* **88**, 075133 (2013), arXiv:1305.1894.
- [55] M. Henkel, *Conformal Invariance and Critical Phenomena* (Springer, New York, 1999).
- [56] F. Verstraete and J. I. Cirac, *Phys. Rev. B* **73**, 094423 (2006).
- [57] F. Verstraete, D. Porras, and J. I. Cirac, *Phys. Rev. Lett.* **93**, (2004), arXiv:cond-mat/0404706.
- [58] P. Pippin, S. R. White, and H. G. Evertz, *Phys. Rev. B* **81**, 081103 (2010).
- [59] J. Haegeman, J. I. Cirac, T. J. Osborne, I. Pižorn, H. Verschelde, and F. Verstraete, *Phys. Rev. Lett.* **107**, 070601 (2011), arXiv:1103.0936.

## Supplemental Material

### puMPS gradient descent

A puMPS on  $N$  sites is defined as

$$|\Psi(A)\rangle = \sum_{\vec{s}=1}^d \text{Tr}(A^{i_1} A^{i_2} \dots A^{i_N}) |\vec{s}\rangle.$$

This explicitly translation invariant ansatz serves as the variational ansatz for ground state of translation invariant spin chains. In contrast to infinite MPS as an ansatz for thermodynamic critical spin chains, where long range physics is not captured, puMPS on a finite circle can have high fidelity with the true ground state, given that bond dimension grows in polynomial with system size [56].

Optimization of periodic MPS, which typically costs  $\mathcal{O}(ND^5)$  or higher, is known to be numerically more costly than open boundary MPS [57, 58], especially when translation invariance needs to be kept explicitly. By truncating singular values of the transfer matrix one can reduce the cost to  $\mathcal{O}(ND^3)$ , but it is not applicable to critical systems [34]. Here, we propose a local gradient descent method that takes advantage of both time dependent variational principle (TDVP) [34, 59] and local gradient descent for open boundary MPS [31].

The energy minimization goes as follows. First, transform the puMPS into the *central gauge* analogous to that of the open boundary MPS case [24]. We express the MPS tensor  $A$  as  $A_C \lambda^{-1}$ , where  $\lambda$  is a  $D \times D$  diagonal matrix and  $A_C$  is a  $d \times D \times D$  tensor. They are chosen such that

$$A_L = A_C \lambda^{-1} \quad A_R = \lambda^{-1} A_C$$

satisfy left and right canonical condition, respectively

$$\sum_i A_L^{\dagger i} A_L^i = a \mathbf{1},$$

$$\sum_i A_R^i A_R^{\dagger i} = a \mathbf{1}.$$

The proportionality constant  $a$  is chosen such that the puMPS state is normalized. This local regauging of MPS does not depend on the boundary conditions, and thus can be done in the same way as the open boundary MPS case. The difference is that, in the case of open boundary MPS,  $a = 1$  ensures the normalization of the state, while in puMPS it is generally not true. Then the energy functional can be written as a function of  $\lambda$  and  $A_C$ ,

$$E(\lambda, A_C, \bar{A}_C) = \frac{\langle \Psi(\lambda, \bar{A}_C) | H | \Psi(\lambda, A_C) \rangle}{\langle \Psi(\lambda, \bar{A}_C) | \Psi(\lambda, A_C) \rangle},$$

where we treat  $A_C$  and its complex conjugate as independent parameters. For compactness, we denote the components of tensor  $A_C$  as  $A_C^\mu$ , where  $\mu = 1, 2 \dots dD^2$  is the

joint index of physical index and bond indices for tensor  $A_C$ . To minimize the energy functional, we compute the local gradient of the energy functional,  $\partial E / \partial \bar{A}_C^\mu$ , where the derivative is taken with respect to  $A_C$  on only *one site*, say, the  $N$ th site. The result does not depend on the site where the derivative is taken as a result of translation invariance. In contrast to MPS with open boundary condition, the derivative is not the optimal direction for the tensor  $A_C$  to move, because the variational manifold is not flat [31, 59]. Instead, the variational manifold is equipped with a Kähler metric  $g_{\bar{\mu}\nu}$ , which in our case is the local effective norm matrix,

$$g_{\bar{\mu}\nu}(\lambda, A_C, \bar{A}_C) = \left\langle \frac{\partial}{\partial \bar{A}_C^\nu} \Psi \left| \frac{\partial}{\partial A_C^\mu} \Psi \right. \right\rangle, \quad (6)$$

where the derivatives are taken with respect to the tensor on the *same* site. Then the local gradient descent direction becomes

$$\Delta A_C^\mu = g^{\mu\bar{\nu}} \frac{\partial E}{\partial \bar{A}_C^\nu}, \quad (7)$$

where  $g^{\mu\bar{\nu}}$  is the inverse of the metric, satisfying  $g^{\mu\bar{\nu}} g_{\bar{\nu}\rho} = \delta_\rho^\mu$ .

Now we are ready to compute the optimal gradient with tensor networks. The local metric  $g_{\bar{\mu}\nu}$  is represented in Fig. 5. The derivative  $\partial E / \partial \bar{A}_C^\nu$  can be further simplified with following trick:

$$\begin{aligned} \frac{\partial E}{\partial \bar{A}_C^\nu} &= \frac{\langle (\partial / \partial \bar{A}_C^\nu) \Psi(\bar{A}) | H | \Psi(A) \rangle}{\langle \Psi(\bar{A}) | \Psi(A) \rangle} \\ &\quad - \frac{\langle \Psi(\bar{A}) | H | \Psi(A) \rangle}{\langle \Psi(\bar{A}) | \Psi(A) \rangle^2} \langle (\partial / \partial \bar{A}_C^\nu) \Psi(\bar{A}) | \Psi(A) \rangle. \end{aligned}$$

The second term can be eliminated by requiring that at each iterative step the expectation of energy is zero, which can be achieved by a shift of Hamiltonian  $\tilde{H} = H - \langle H \rangle$ . Thus,

$$\frac{\partial E}{\partial \bar{A}_C^\nu} = \frac{\langle (\partial / \partial \bar{A}_C^\nu) \Psi(\bar{A}) | \tilde{H} | \Psi(A) \rangle}{\langle \Psi(\bar{A}) | \Psi(A) \rangle}. \quad (9)$$

The shift of Hamiltonian does not alter the ground state, which justifies above simplification. The derivative in (9) is represented as tensor networks in Fig. 5.

Defining  $\Delta A_L^\mu \equiv A_C^\mu \lambda^{-1}$ , we update the state as

$$A'^\mu = A_L^\mu - \alpha \Delta A_L^\mu,$$

where  $\alpha$  is the step size obtained by either line search or empirical adjustment.  $A'$  is then used as the new puMPS tensor (for all sites), resulting in an updated state. Since  $A'$  is generally no longer in a canonical form, we may then transformed the updated puMPS back into, say, left canonical form.

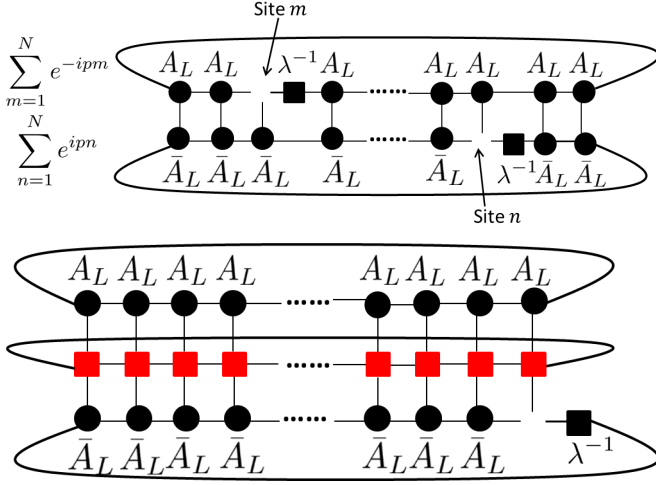


Figure 5. Top: the tensor network for the local effective norm matrix (6) in central gauge. Bottom: the tensor network for the derivative of energy functional with respect to the puMPS tensor  $A_C$  in (9).

The convergence is monitored by the norm of the local gradient. It is defined as

$$\eta = \sqrt{g^{\mu\bar{\nu}} \frac{\partial E}{\partial A_C^\mu} \frac{\partial E}{\partial \bar{A}_C^\nu}},$$

and is analogous to the convergence measure used in the TDVP. We usually stop the iteration when  $\eta < 10^{-6}$ .

The numerical cost for each iterative step is  $\mathcal{O}(ND^5)$ . The main difference from TDVP is that in the latter method the full effective norm matrix is computed, i.e., the derivative in (6) is taken with respect to the tensor on *all* sites, which costs  $\mathcal{O}(ND^6)$ .

Unlike the case of open boundary MPS, where the use of central canonical form immediately takes the local effective norm matrix to be identity, the local metric  $g_{\bar{\mu}\nu}$  is nontrivial due to periodic boundary condition. The inverse metric, however, does not need to be computed densely, since all we need is to compute (7), where the left hand side can be solved iteratively from the linear equation. The use of central gauge, though it does not eliminate the need for inverting the metric, is necessary in practice, since it generally leads to a better conditioned local metric favored by iterative linear equation solvers.

### Preconditioning of puMPS

Optimization algorithm using gradient descent usually suffers from local minimums. *Preconditioning* serves as a procedure to find a initial state that approximates the global minimum, with which gradient descent works better. In the context of puMPS optimization, we observe that starting with a random state usually works for

smaller bond dimension in smaller systems. For puMPS with larger bond dimension in larger systems, the energy landscape of the variational manifold becomes more complicated, and the algorithm is more likely to be stuck in a local minimum. Here, we use several simple ways of preconditioning.

First, we can directly use the optimized puMPS tensor for system size  $N_0$  as the building block for the initial state for slightly larger system sizes  $N_1 > N_0$  with the same bond dimension.

Second, for the same system, to find an initial puMPS state with bond dimension  $D_1$ , we can use the optimized puMPS tensor with smaller bond dimension  $D_0$ , enlarging it to  $d \times D_1 \times D_1$  and filling the vacancies with small random numbers.

We compare the convergence of local gradient descent algorithm in two cases: with preconditioning or starting with random state, see Fig. 6. The result shows that preconditioning significantly accelerates convergence and helps producing more accurate ground state approximation with puMPS.

### Excited state ansatz

The excited state ansatz with momentum  $p$  is a tangent vector of optimized puMPS, also known as a Bloch state,

$$|\Phi_p(B, A)\rangle = \sum_{n=1}^N e^{-ipn} T^j \sum_{\bar{s}=1}^d \text{Tr}(B^{s_1} A^{s_2} \dots A^{s_N}) |\bar{s}\rangle. \quad (10)$$

The Hamiltonian eigenvalue equation in the subspace of tangent vectors is then transformed into a generalized eigenvalue equation [25]

$$H_{\bar{\mu}\nu}(p) B^\nu = E N_{\bar{\mu}\nu}(p) B^\nu, \quad (11)$$

where  $N_{\bar{\mu}\nu}(p)$ ,  $H_{\bar{\mu}\nu}(p)$  are effective norm matrix and effective Hamiltonian for tangent vectors in each momentum sector, defined as

$$N_{\bar{\mu}\nu}(p) = \left\langle \frac{\partial}{\partial \bar{B}^\mu} \Phi_p(B, A) \left| \frac{\partial}{\partial B^\nu} \Phi_p(B, A) \right\rangle$$

$$H_{\bar{\mu}\nu}(p) = \left\langle \frac{\partial}{\partial \bar{B}^\mu} \Phi_p(B, A) \left| H \left| \frac{\partial}{\partial B^\nu} \Phi_p(B, A) \right\rangle,\right.$$

where the derivative is taken with respect to the tensor on *all* sites as opposed to the local metric in ground state optimization.

We have to be a bit cautious when solving the generalized eigenvalue equation (11), since the full effective norm matrix  $N_{\bar{\mu}\nu}(p)$  is only semi-positive definite due to gauge freedom of MPS tangent vectors [34, 54]. Even if we project out its null space, it is still not well conditioned as many positive eigenvalues may be close to zero. The first problem is settled if we use the pseudoinverse of the effective norm matrix instead of ordinary inverse. To solve the second problem, we can again resort

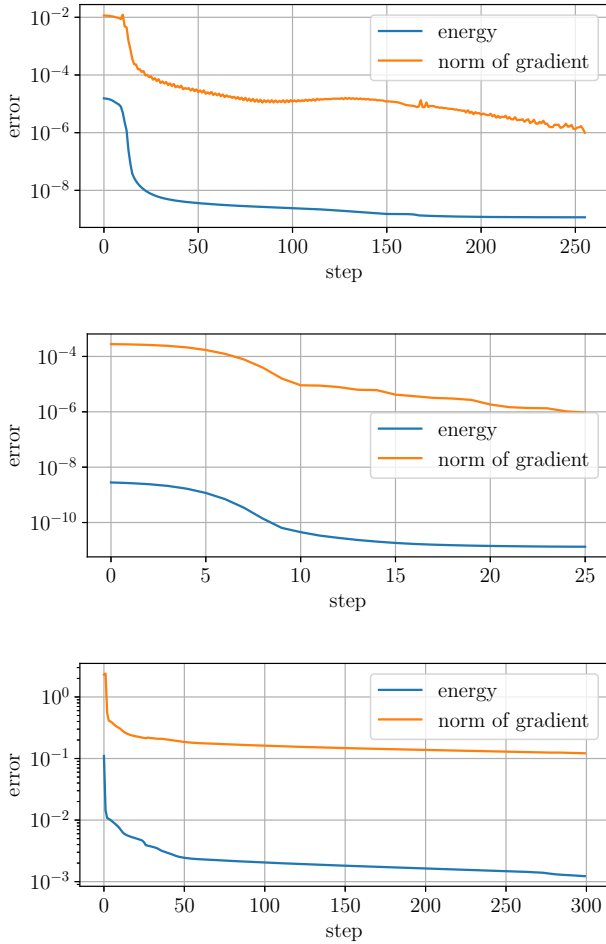


Figure 6. Convergence of the puMPS gradient descent algorithm with preconditioning for the Ising model with  $N = 128$ . The orange curve is the convergence of gradient norm  $\eta$ , and the blue curve represents the energy difference of puMPS from the analytic ground state energy at each step of energy minimization. Top: Bond dimension  $D = 18$ , initial state chosen with the pre-optimized puMPS tensor for  $N = 64, D = 18$ . Middle: Bond dimension  $D = 30$ , initial state chosen by enlarging the optimized puMPS tensor from  $D = 18, N = 128$ . Bottom: Bond dimension  $D = 30$ , starting with a random state.

to the central gauge, where the puMPS tangent vector is parametrized by  $A_L = A_C \lambda^{-1}$  and  $B_C = B \lambda$ . Then (11) can be rewritten in terms of  $B_C$ ,

$$H_{\bar{\mu}\nu,C}(p)B_C^\nu = EN_{\bar{\mu}\nu,C}(p)B_C^\nu, \quad (14)$$

where  $N_{\bar{\mu}\nu,C}(p)$  and  $H_{\bar{\mu}\nu,C}(p)$  are obtained by substituting the derivatives in (12), (13) by derivatives with respect to  $B_C$ . They are depicted as tensor networks in Fig. 7.

The effective norm matrix  $N_{\bar{\mu}\nu,C}(p)$  in central gauge is much better conditioned than the original effective norm matrix  $N_{\bar{\mu}\nu}(p)$ . We plot their eigenvalues for the Ising model with  $N = 64$  and puMPS bond dimension  $D = 24$

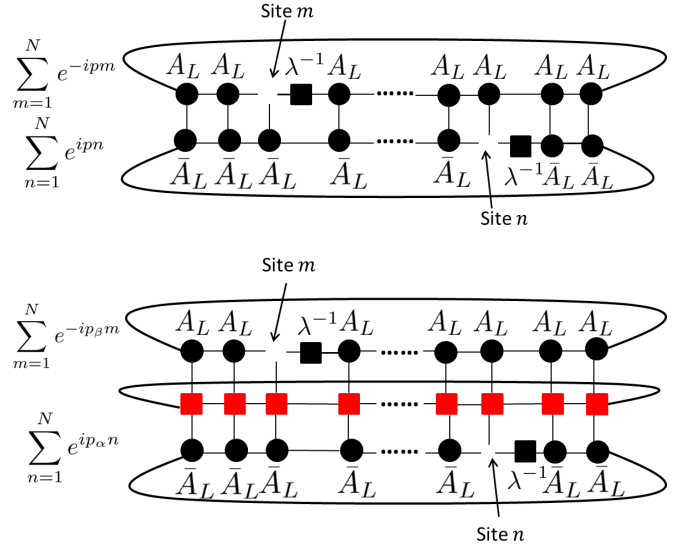


Figure 7. Top: the tensor network for the effective norm matrix  $N_{\bar{\mu}\nu,C}$  in central gauge. Bottom: the tensor network for effective Hamiltonian ( $p_\alpha = p_\beta = p$ ) and effective  $H_n$  matrices in central gauge, where the red tensors in the middle form a MPO representation of Hamiltonian and its Fourier modes, respectively.

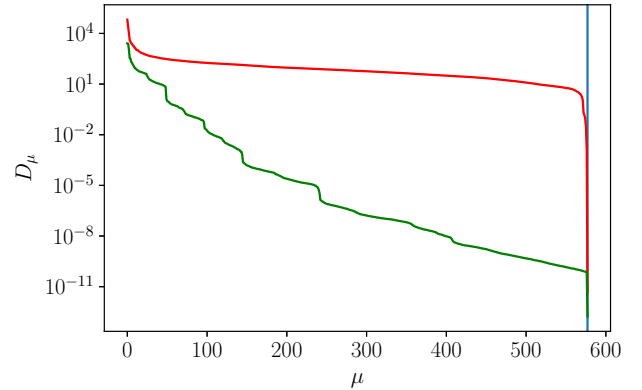


Figure 8. Nonzero eigenvalues  $D_\mu$  of the effective norm matrix in momentum zero sector of the Ising model with  $N = 64, D = 24$ , sorted in descending order. Red:  $N_{\bar{\mu}\nu,C}(p = 0)$  in the central gauge. Green:  $N_{\bar{\mu}\nu}(p = 0)$  in the left canonical gauge. The blue vertical line is at  $\mu = (d-1)D^2 + 1$ , the number of nonzero eigenvalues resulting from the gauge freedom of puMPS tangent vectors in momentum zero sector.

to show it explicitly, see Fig. 8.

We multiply the *pseudoinverse*  $\tilde{N}_C^{\rho\bar{\mu}}(p)$  of the effective norm matrix on both sides of (14) to obtain the ordinary eigenvalue equation,

$$\tilde{N}_C^{\rho\bar{\mu}}(p)H_{\bar{\mu}\nu,C}(p)B_C^\nu = EB_C^\rho. \quad (15)$$

Finally we solve (15) by the usual Lanczos algorithm, and multiply  $B_C$  by  $\lambda$  to get back to  $B$ . For each momentum



sector, only a few eigenstates are computed, since the tangent vector ansatz is only capable of approximating the low energy spectrum.

The computation of  $N_{\bar{\mu}\nu,C}(p)$  and  $H_{\bar{\mu}\nu,C}(p)$  costs  $\mathcal{O}(ND^6)$ . However, since we only need to construct the matrices only once for each momentum sector, the actual time cost is usually less than ground state optimization.

### Fidelity with Exact Diagonalization

We explicitly check the fidelity of puMPS tangent vectors obtained above with eigenstates obtained by exact diagonalization for the Ising model with  $N = 20$ . The fidelity is defined as

$$f = \langle \Phi_{p_\alpha}(B_\alpha, A) | \Phi_{\alpha,ED} \rangle,$$

where  $|\Phi_{\alpha,ED}\rangle$  is the  $\alpha$ th eigenstate from diagonalizing the Hamiltonian, and  $\Phi_{p_\alpha}(B_\alpha, A)$  is the corresponding eigenstate represented by puMPS tangent vector with momentum  $p_\alpha$ . We compute the first 41 eigenstates corresponding to the first 4 levels of conformal towers ( $\Delta \leq 4 + 1/8$ ). The result is shown in Fig. 9.

We can see that although fidelity decreases as energy increases for a fixed bond dimension, fidelity increases uniformly for each state as the bond dimension increases, regardless of energy and conformal tower of the state. Then we conclude that the puMPS tangent vector ansatz, (10), can capture all eigenstates in the low energy spectrum with sufficiently small errors given large enough bond dimension.

### Computation of matrix elements of Virasoro generators

The Virasoro generators are constructed as Fourier modes of Hamiltonian, see the main text. The zero mode  $H_0$  is the Hamiltonian itself, while  $H_n = H_{-n}^\dagger$  are ladder operators that connect different states in the same conformal tower. For the purpose of identifying conformal towers, it suffices to compute the matrix elements of  $H_1$  and  $H_2$  in low energy basis,

$$H_{n,\alpha\beta} = \langle \Phi_{p_\alpha}(\bar{B}_\alpha, \bar{A}) | H_n | \Phi_{p_\beta}(B_\beta, A) \rangle, \quad (16)$$

where  $\alpha$  and  $\beta$  are labels for eigenstates in low energy spectrum. It is nonzero only if the momenta match, i.e.,

$$p_\alpha + 2\pi n/N = p_\beta. \quad (17)$$

(16) is obviously bilinear in the  $B$  tensors, thus we can define the effective  $H_n$  matrix  $H_{n,\bar{\mu}\nu}$  implicitly as

$$\bar{B}_\alpha^\mu H_{n,\bar{\mu}\nu}(p_\alpha, p_\beta) B_\beta^\nu = H_{n,\alpha\beta}, \quad (18)$$

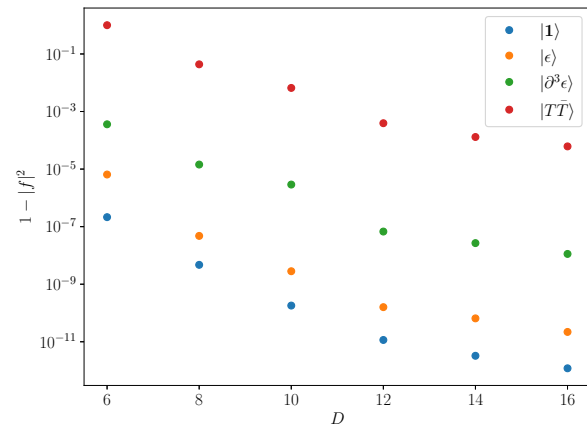
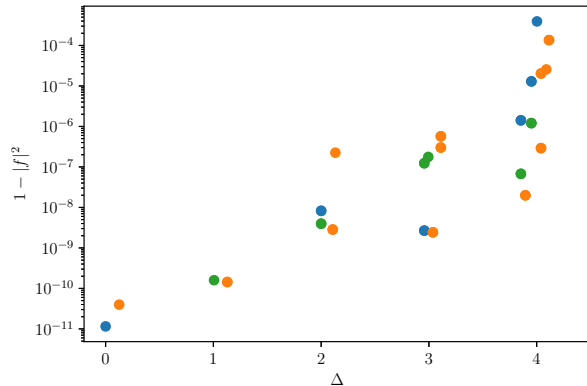


Figure 9. Fidelity of the first 41 states of puMPS tangent vectors with exactly diagonalized eigenstates of the Ising model with  $N = 20$ . Top: fidelity of all 41 states for fixed bond dimension  $D = 12$ . Different colors label states in different conformal towers. Bottom: fidelity of four states for bond dimensions  $6 \leq D \leq 16$ . All ground states are converged to  $\eta < 10^{-6}$ .

where  $\mu, \nu$  are indices of the  $B$  tensors. When  $n = 0$  and  $p_\alpha = p_\beta = p$ ,  $H_{n,\bar{\mu}\nu}(p_\alpha, p_\beta)$  reduces to the effective Hamiltonian  $H_{\bar{\mu}\nu}(p)$  in (13). The computation of effective  $H_n$  matrices is also similar to that of the effective Hamiltonian. The only difference is that we need to change phases of certain elements in the MPO, see Fig. 7. Thus, for each  $n$  and each pair of momenta satisfying (17), the computation cost is also  $\mathcal{O}(ND^6)$ . Finally, we can plug into (18) the tangent state  $B$  tensors to obtain the matrix elements  $H_{n,\alpha\beta}$  of  $H_n$  in the low energy basis with a negligible  $\mathcal{O}(D^2)$  cost.

### Identification of conformal towers

With the help of matrix elements of ladder operators  $H_n$ , we may identify conformal towers following the method in [12]. Here, we propose a slightly different ap-

proach which identifies conformal towers level by level.

First, we identify primary states following method in [12]. Denote the number of primary states as  $n_p$ . Then, for each state  $|\Phi_\alpha\rangle$ , assign an array  $C_{\alpha l}$ , where  $l = 1, 2 \cdots n_p$ . For primary states,  $C_{\alpha l} = \delta_{l, l_0}$ , where  $l_0$  is the index for the primary state. Next, for non-primary states, from energy lower to higher, compute

$$C_{\alpha l} = \sum_{n=-2}^{+2} \sum_{E_\beta < E_\alpha} |H_{n, \alpha\beta}|^2 C_{\beta l},$$

and normalize the array  $C_{\alpha l}$ . Finally, determine for each non-primary state which conformal tower it belongs to, according to which component of  $C_{\alpha l}$  is the largest.

Typically, the largest component of  $C_{\alpha l}$  decays with energy resulting from finite size effect. However, for the Ising model, we find that the finite size effect causes little problem in conformal tower identification for low lying spectrum, where finite bond dimension effect is not strong. This is in accordance with [12], which results from the fact that finite size perturbation for the Ising model comes from operators in the identity tower.

#### Extrapolation of conformal data

As mentioned in the main text, scaling dimensions  $\Delta_\alpha$  and conformal spin  $s_\alpha$  are extracted from the energy-

momentum spectrum, and the central charge  $c$  is extracted from the matrix element of  $H_2$ . There are non-universal finite size corrections to  $\Delta_\alpha$  and  $c$  at finite system sizes, which depends on particular lattice realization of CFT. By collecting  $\Delta_\alpha$  and  $c$  for different system sizes and extrapolating to the thermodynamic limit, we can obtain conformal data with higher accuracy.

Physical quantities near CFT usually exhibit power law scaling. In general, we can relate the finite size conformal data  $\Delta_\alpha(N), c(N)$  to their thermodynamic value  $\Delta_\alpha, c$  by

$$\begin{aligned} \Delta_\alpha(N) &= \Delta_\alpha + \frac{b_\alpha}{N^{x_\alpha}} + \mathcal{O}(N^{-x_\alpha}) \\ c(N) &= c + \frac{b_c}{N^{x_c}} + \mathcal{O}(N^{-x_c}), \end{aligned}$$

where  $\mathcal{O}()$  terms stand for higher order non-universal corrections. For the Ising model,  $x_\alpha = x_c = 2$  due to the presence of perturbation of operators at level 4. Then we can linearly fit finite size conformal data with  $N^{-2}$  to extrapolate the thermodynamic quantities, see Fig. 10.

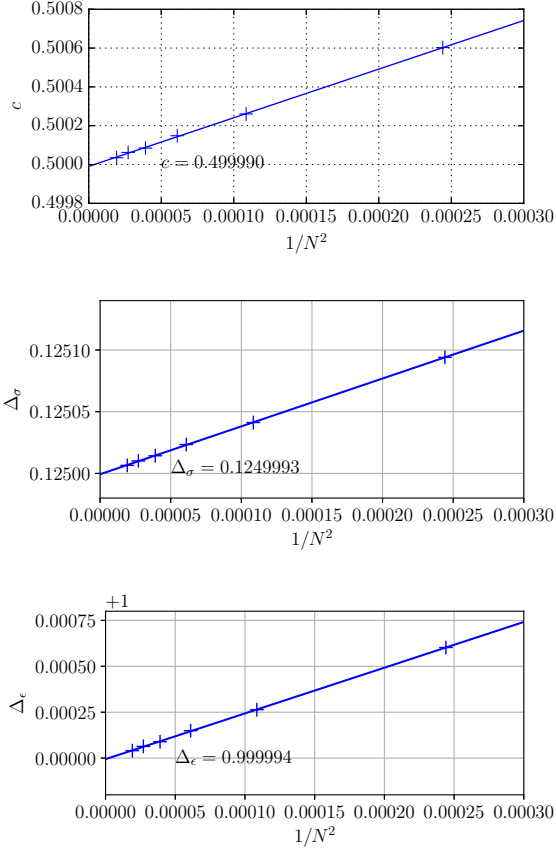


Figure 10. Extrapolation of scaling dimensions of primary fields and central charge for the Ising CFT with finite size simulations of the Ising model. Data points include  $N = 64, 96, 128, 160, 192, 228$  with bond dimension  $N = 24, 24, 30, 30, 36, 36$  respectively. The bond dimensions are chosen such that error in ground state energy is less than  $10^{-10}$ .